IEEE Access
Multidisciplinary | Rapid Review | Open Access Journal

Received 18 March 2024, accepted 1 April 2024, date of publication 10 April 2024, date of current version 17 April 2024.

Digital Object Identifier 10.1109/ACCESS.2024.3386855

RESEARCH ARTICLE

Stability-Enhanced Model Predictive Control for Urban Rail Transit Train

XI WANG[1], KEJIA XING[2], AND JIAN WANG[1,2]
[1]Postgraduate Department, China Academy of Railway Sciences, Beijing 100081, China
[2]Signal and Communication Research Institute, China Academy of Railway Sciences Corporation Ltd., Beijing 100081, China

Corresponding author: Kejia Xing (xingkejia@rails.cn)

This work was supported in part by the National Natural Science Foundation of China under Grant 52172323, and in part by China Academy of Railway Sciences Fund under Grant 2021YJ305.

ABSTRACT Automatic train operation (ATO) control is a pivotal part of urban rail transit development, where designing the dynamics models and controllers for the ATO control scenarios presents a formidable challenge. To begin with, considering the fundamental resistances encountered by trains during the operation process, including elemental running resistance and time-varying slope resistance, we treat relative distance and relative speed between train carriages as state variables in the control modeling. Considering changes in traction/braking outputs as control variables, we formulate a meticulous dynamics model for urban rail transit trains (URTT). Furthermore, a stability-enhanced model predictive control (SEMPC) approach is proposed for ATO control in URTT, with a terminal term being added to the control objective design for stability requirements. This approach anticipates the future dynamic behaviors of the control system, yielding a stable and convergent predictive controller for the ATO system. Lastly, utilizing operational data from a specific urban rail line as an illustrative example, we conduct comparative analyses of the operational control performance among various controllers in scenarios of the single section, multi-section, and disturbance. Experimental results demonstrate that the proposed SEMPC controller exhibits superior performance to the compared controllers in terms of input cost, speed error, displacement error, and station-stopping error for ATO control in URTT.

INDEX TERMS Automatic train operation (ATO), urban rail transit train (URTT), stability-enhanced model predictive control (SEMPC), speed control.

I. INTRODUCTION

With the development of urban clusters and metropolitan areas, the demand for constructing an efficient and reliable urban rail transit train (URTT) system is rapidly increasing, where an indispensable component is the automatic train operation (ATO) control responsible for train speed control and station stopping [1]. Specifically speaking, ATO control technology is achieved by adjusting the traction and braking control commands for the train, tracking the target speed profile within speed limits, and coming to a precise stop within the stopping window (station stopping point $\pm$ 0.3 m), thereby guaranteeing safe, efficient, and smooth train operation [2]. However, URTT exhibits more complicated operation states during travel in increasingly complex track conditions and operational scenarios, such as higher speed requirements, complex slope variations, and tight stopping windows. This complexity affects the safety, stability, and stopping precision of the train, imposing high requirements on train operation control technology [3]. Thus, it is imperative to establish an accurate train dynamics model and design a train operation control algorithm that adheres to train operation constraints to the demands of speed control and precise station stopping.

In general, the train dynamics model can be categorized into single-point train model and multi-point train model. Compared with the former, the latter treats each train carriage as an individual point, considering coupling relationships between carriages and analyzing the forces acting on each carriage [4]. Hence, the multi-point train model can be more effective in characterizing the dynamic behavior of trains and

The associate editor coordinating the review of this manuscript and approving it for publication was Shaohua Wan.

is widely used in ATO control under complex conditions [5], [6], [7]. For example, a multi-point train model connected by flexible couplers is constructed in [5], which can be cruise control for trains. In [6], it is presented a nonlinear multi-point train model based on integer variables that can represent carriage types and operation states. He et al. [7] devise a robust control criterion applicable to the multi-point train model. This criterion explicitly incorporates the train operation process's uncertainties.

After building the train dynamics model, it is necessary to design the ATO control algorithm. In recent years, a lot of ATO control algorithms have been designed. Among them, proportional-integral-derivative (PID) control has been widely used due to its simplicity [8], [9]. Other intelligent control algorithms, such as expert systems and reinforcement learning [10], [11], [12], [13], event-triggered consensus control [14], sliding mode control (SMC) [15], [16], [17], adaptive fuzzy sliding mode control (AFSMC) [18], and iterative learning control [19], [20], [21], have also been explored. All the above algorithms improve the performance of the train control from the perspective of ATO control. On the other hand, some frontier technologies including blockchain and edge intelligence have been introduced to enhance the performance of the train [22], [23], [24].

However, some of the above control algorithms are limited to optimizing single objectives, lacking the capability to address multi-objective optimization and multiple constraint problems [25], [26], [27]. Considering the nonlinear characteristics of the train operation, the impact of traction motor saturation, riding comfort, various train speed limitations in different sections, and constraints on train speed and stopping positions in different segments, the design of control algorithms needs to consider multiple objectives and constraints. Therefore, in recent years, model predictive control (MPC) algorithms that can effectively handle optimization control problems with complex constraints have received widespread attention [28], [29], [30]. For example, a distributed optimal control for multiple train operations is designed, which overcomes communication constraints and realizes efficient speed control [31].

Simultaneously, considering train operation control's reliability and real-time performance, efficient control algorithms are crucial [32]. Regarding predictive control optimization algorithms, an MPC algorithm considering multiple performance indicators and constraints is introduced to reduce energy waste and alleviate train periodic vibrations in [33]. In [34], a constraint-tightening-based MPC algorithm is presented, achieving speed tracking within the automatic train protection (ATP) limits. A switching cost function MPC algorithm is investigated [35], which switches cost functions in the train control problem based on operation demands. Besides, an MPC algorithm based on a data-driven Koopman model is developed, which completes higher tracking accuracy and control requirements [36]. Furthermore, in terms of station parking, Zhao et al. devise a precise stopping control model based on a distributed MPC algorithm, achieving an accurate and stable station stopping [37].

It is noted that the above MPC algorithms choose train traction/braking output as the control variable for achieving ATO control without taking into account the variation of traction/braking output related to riding comfort. As a consequence, this paper proposes a stability-enhanced model predictive control (SEMPC) approach for ATO control in URTT considering various train operation constraints. Further, the proposed SEMPC approach is validated via experiments, which demonstrate that the proposed SEMPC approach ensures precise train speed control and station stopping control while preserving carriage-to-carriage safety distance and speed under the premise of meeting the requirements for the train's stopping position, speed limit, the input constraints of the vehicle's traction/braking actuators, and riding comfort. The framework of the SEMPC for ATO control in URTT is shown in Fig. 1.

The rest of this paper is organized as follows: Section II presents a multi-point train dynamics model; Section III introduces the proposed SEMPC controller design for ATO; Section IV provides simulation test results and corresponding analysis; Section V summarizes the entire paper.The contributions of this paper are as follows:

- Under the elemental running resistance and the variable slope resistance of trains, this paper considers relative distance and relative speed between train carriages as variable states, by introducing changes in traction/braking output as optimization variables, a dynamics model for URTT is established.
- In this paper, the proposed SEMPC approach sets the tracking performance of expected speed and displacement profiles, maintaining distance safety and speed synchronization between train carriages, and ensuring smooth variations in control variables as control objectives. Furthermore, by introducing a terminal cost function and combining it with complex operational constraints, an SEMPC approach for URTT is derived.
- Using operational data from a specific urban rail line, the performance of different control algorithms is compared in both single-section and multi-section operational scenarios. Experimental results demonstrate that, in comparison with other advanced control algorithms, the proposed SEMPC approach exhibits superior performance.

II. TRAIN DYNAMICS MODEL

Considering the combined influence of traction, braking, and resistance during the train's operation, each carriage is viewed as an individual point. Furthermore, assuming that each carriage of the train can be independently controlled and that different carriages follow corresponding trajectories, the dynamical equations for a train with n carriages can be

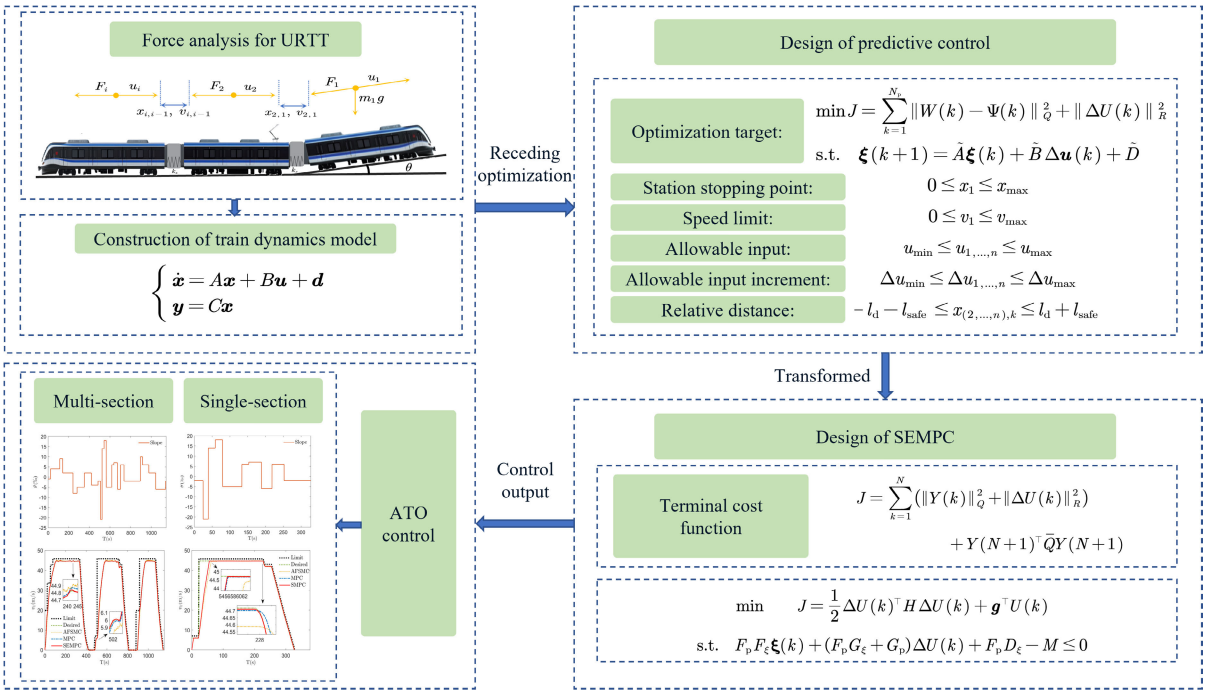

FIGURE 1. Framework of the stability-enhanced model predictive control for urban rail transit trains.

described as follows [31]:

$$\begin{cases} x_i & = v_i, i = 1, \dots, n, \\ m_1 \dot{v}_1 & = u_1 - k_s (x_1 - x_2 - l) - F_1, \\ m_i \dot{v}_i & = u_i + k_s (x_{i-1} - x_i - l) \\ & \quad - k_s (x_i - x_{i+1} - l) - F_i, i = 2, \dots, n-1, \\ m_n \dot{v}_n & = u_n + k_s (x_{n-1} - x_n - l) - F_n, \end{cases} \tag{1}$$

where u_i signifie the traction force experienced by the i-th carriage, m_i stands for the mass of the i-th carriage, and x_i and v_i represent the position and speed of the i-th carriage, respectively. In addition, l denotes the original length of the spring and k_s represents the linear spring stiffness coefficient.

In the technical development of the ATO system for URTT, the ATO control algorithm considers the influence of the elemental running resistance and the slope resistance on the train. Hence, F_i represents the resistance experienced by the i-th carriage, specifically given by $F_i = F_r^i + F_w^i$. The elemental running resistance and the slope resistance of the i-th carriage as follow [3]:

$$F_r^i = m_i \left(c_0 + c_1 v_i + c_2 v_i^2 \right), \tag{2}$$

$$F_w^i = m_i w_i = m_i \cdot g \cdot \theta \cdot 10^{-3}, \tag{3}$$

where c_0, c_1, and c_2 are the Davis' coefficients, which are decided by the type of train. In (3), w_i represents the unit slope resistance, g is the acceleration due to gravity, and θ represents the slope in permillage (positive for uphill) [38].

In order to ensure the safe distance and speed synchronization between carriages, we assume $x_{i,i-1} = x_i - x_{i-1}$ and $v_{i,i-1} = v_i - v_{i-1}$, and take it as the variable of states, then substitute it into (1). Thus, we get the error dynamics equation as follows:

$$\begin{cases} \dot{x}_1 & = v_1, \\ \dot{x}_{i,i-1} & = v_{i,i-1}, i = 2, \dots, n, \\ \dot{v}_1 & = \dfrac{u_1}{m_1} - \dfrac{k}{m_1}\left(-x_{2,1} - l\right) - F_1, i = 1, \\ \dot{v}_{2,1} & = \dfrac{u_2}{m_2} + \dfrac{k}{m_2}\left(-x_{2,1} - l\right) \\ & \quad - \dfrac{k}{m_2}\left(-x_{3,2} - l\right) - F_2 \\ & \quad - \dfrac{u_1}{m_1} + \dfrac{k}{m_1}\left(-x_{2,1} - l\right) + F_1, i = 2, \\ \dot{v}_{i,i-1} & = \dfrac{u_i}{m_i} + \dfrac{k}{m_i}\left(-x_{i,i-1} - l\right) \\ & \quad - \dfrac{k}{m_i}\left(-x_{i+1,i} - l\right) - F_i \\ & \quad - \dfrac{u_{i-1}}{m_{i-1}} - \dfrac{k}{m_{i-1}}\left(-x_{i-1,i-2} - l\right) \\ & \quad + \dfrac{k}{m_{i-1}}\left(-x_{i,i-1} - l\right) + F_{i-1}, \ i = 3, \dots, n-1, \\ \dot{v}_{n,n-1} & = \dfrac{u_n}{m_n} + \dfrac{k}{m_n}\left(-x_{n,n-1} - l\right) - F_n \\ & \quad - \dfrac{u_{n-1}}{m_{n-1}} - \dfrac{k}{m_{n-1}}\left(-x_{n-1,n-2} - l\right) \\ & \quad + \dfrac{k}{m_{n-1}}\left(-x_{n,n-1} - l\right) + F_{n-1}, i = n, \end{cases} \tag{4}$$

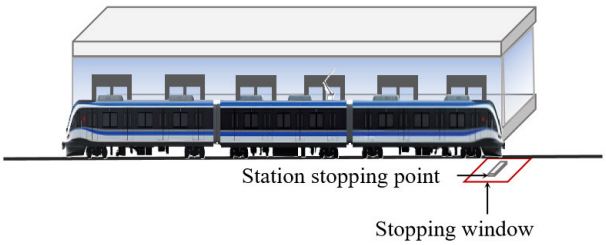

(a) The diagram of station stopping.

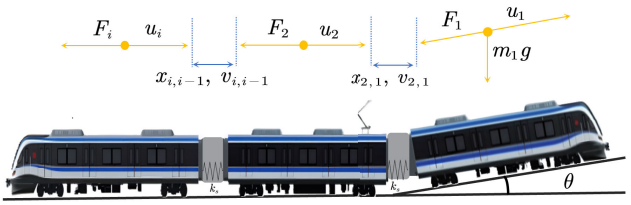

(b) Force condition of the urban rail transit train.

FIGURE 2. The diagram of (a) station stopping and (b) force condition for URTT.

where $v_{i,i-1}$ represents the relative speed of the i-th carriage concerning the $(i-1)$-th carriage, and $x_{i,i-1}$ denotes the relative distance of each carriage behind it. The diagram of station stopping is shown in Fig. 2(a) and the multi-point train model is illustrated in Fig. 2(b).

Due to the presence of high-order terms concerning speed v_i, a linearization method [39] is employed to approximate the high-order terms of v_i with a first-order Taylor approximation at t. Here, v_r represents the reference speed of the train at time t. In other words, the high-order terms of v_i are approximated linearly around the point t.

$$v_i^2 \approx v_r^2 + 2v_r(v_i - v_r) = 2v_r v_i - v_r^2.$$

Furthermore, assuming equal masses for each carriage, the continuous system state-space equations describing the motion of the train can be formulated as follows:

$$\begin{cases} \dot{\boldsymbol{x}} = A\boldsymbol{x} + B\boldsymbol{u} + \boldsymbol{d}, \\ \boldsymbol{y} = C\boldsymbol{x}, \end{cases} \tag{5}$$

where $\boldsymbol{y}$ is the output of the control system,

$$\boldsymbol{x} = \begin{bmatrix} x_1 \\ \vdots \\ x_{n,n-1} \\ v_1 \\ \vdots \\ v_{n,n-1} \end{bmatrix}, \quad \boldsymbol{u} = \begin{bmatrix} u_1 \\ \vdots \\ u_n \end{bmatrix}, \quad \boldsymbol{y} = \begin{bmatrix} y_{x_1} \\ \vdots \\ y_{x_{n,n-1}} \\ y_{v_1} \\ \vdots \\ y_{v_{n,n-1}} \end{bmatrix}.$$

The expressions for matrices A, B, C, and $\boldsymbol{d}$ are as follows:

$$A = \begin{bmatrix} A_{11} & A_{12} \\ A_{21} & A_{22} \end{bmatrix}_{2n\times 2n},$$

$$B = \begin{bmatrix} \frac{1}{m} & 0 & 0 & \cdots & 0 \\ -\frac{1}{m} & \frac{1}{m} & 0 & \cdots & 0 \\ 0 & -\frac{1}{m} & \frac{1}{m} & & \\ \vdots & \ddots & \ddots & \ddots & \\ 0 & \cdots & 0 & -\frac{1}{m} & \frac{1}{m} \end{bmatrix}_{2n\times n},$$

$$C = \begin{bmatrix} 1 & \cdots & 0 \\ \vdots & \ddots & \vdots \\ 0 & \cdots & 1 \end{bmatrix}_{2n\times 2n},$$

$$\boldsymbol{d} = \begin{bmatrix} 0 \\ \vdots \\ 0 \\ -c_0 + c_2 v_r^2 + \frac{k_s l}{m} - w_1 \\ w_1 - w_2 - \frac{k_s l}{m} \\ \vdots \\ w_{i-1} - w_i \\ \vdots \\ w_{n-1} - w_n - \frac{k_s l}{m} \end{bmatrix}_{2n\times 1},$$

where

$$A_{11} = \begin{bmatrix} 0 & \cdots & 0 \\ \vdots & \ddots & \vdots \\ 0 & \cdots & 0 \end{bmatrix}_{n\times n},$$

$$A_{12} = \begin{bmatrix} 1 & \cdots & 0 \\ \vdots & \ddots & \vdots \\ 0 & \cdots & 1 \end{bmatrix}_{n\times n},$$

$$A_{21} = \begin{bmatrix} 0 & \frac{k_s}{m} & 0 & \cdots & 0 \\ 0 & -\frac{2k_s}{m} & \ddots & \ddots & \vdots \\ 0 & \frac{k_s}{m} & \ddots & \ddots & 0 \\ \vdots & \ddots & \ddots & \ddots & \frac{k_s}{m} \\ 0 & \cdots & 0 & \frac{k_s}{m} & -\frac{2k_s}{m} \end{bmatrix}_{n\times n},$$

$$A_{22} = \begin{bmatrix} -c_1 - 2c_2 v_\mathrm{r} & 0 & \cdots & 0 \\ 0 & -c_1 - 2c_2 v_\mathrm{r} & \cdots & 0 \\ \vdots & \vdots & \ddots & \vdots \\ 0 & 0 & \cdots & -c_1 - 2c_2 v_\mathrm{r} \end{bmatrix}_{n\times n}.$$

III. CONTROLLER DESIGN FOR ATO

This section contains two subsections. Section III-A introduces the design of predictive control. In Section III-B, the SEMPC approach for URTT is derived.

A. DESIGN OF PREDICTIVE CONTROL

In this subsection, it is divided into three parts. Firstly, the design of the prediction model is introduced. Secondly, the design of the objective function is developed. Finally, the design of constraints is clarified.

1) DESIGN OF PREDICTION MODEL

Generally, optimization can be performed within the prediction horizon in the predictive control algorithm to determine future control actions based on several performance criteria [40]. The continuous state-space equations are transformed into a discrete form by discretizing (5) using the forward Euler method.

$$\begin{cases} \boldsymbol{x}(k+1) = A_{\mathrm{d}}\boldsymbol{x}(k) + B_{\mathrm{d}}\boldsymbol{u}(k) + \boldsymbol{d}, \\ \boldsymbol{y}(k) = C_{\mathrm{d}}\boldsymbol{x}(k), \end{cases} \tag{6}$$

where $A_{\mathrm{d}} = I + AT, B_{\mathrm{d}} = TB, C_{\mathrm{d}} = C$, I represents the identity matrix, and T denotes the sampling period.

Furthermore, considering riding comfort, (6) can be rewritten as a state equation with control increments as inputs:

$$\begin{cases} \boldsymbol{\xi}(k+1) = \tilde{A}\boldsymbol{\xi}(k) + \tilde{B}\Delta\boldsymbol{u}(k) + \tilde{D}, \\ \boldsymbol{\eta}(k) = \tilde{C}\boldsymbol{\xi}(k), \end{cases} \tag{7}$$

where

$$\boldsymbol{\xi}(k) = \begin{bmatrix} \boldsymbol{x}(k) \\ \boldsymbol{u}(k-1) \end{bmatrix}, \quad \Delta\boldsymbol{u}(k) = \begin{bmatrix} \Delta u_1(k) \\ \vdots \\ \Delta u_n(k) \end{bmatrix},$$

$$\boldsymbol{\eta}(k) = \begin{bmatrix} \boldsymbol{y}(k) \\ \boldsymbol{u}(k) \end{bmatrix}, \quad \tilde{A} = \begin{bmatrix} A_{\mathrm{d}} & B_{\mathrm{d}} \\ O_{n\times 2n} & I_{n\times n} \end{bmatrix}, \quad \tilde{B} = \begin{bmatrix} B_{\mathrm{d}} \\ I_{n\times n} \end{bmatrix},$$

$$\tilde{C} = \begin{bmatrix} C_{\mathrm{d}} & O_{n\times n} \\ O_{n\times n} & O_{n\times n} \end{bmatrix}, \quad \tilde{D} = \begin{bmatrix} \boldsymbol{d} \\ O_{n\times 1} \end{bmatrix}.$$

In these equations, O represents the zero matrix. Conducting state prediction based on (7), where N_{c} is the control domain and N_{p} is the prediction domain, it can be described in vector form as

$$\Xi(k) = F_\xi\boldsymbol{\xi}(k) + G_\xi\Delta U(k) + D_\xi, \tag{8}$$

where

$$\Xi(k) = \begin{bmatrix} \boldsymbol{\xi}(k+1) \\ \vdots \\ \boldsymbol{\xi}\left(k+N_{\mathrm{p}}\right) \end{bmatrix}, \quad \Delta U(k) = \begin{bmatrix} \Delta\boldsymbol{u}(k) \\ \vdots \\ \Delta\boldsymbol{u}\left(k+N_{\mathrm{p}}-1\right) \end{bmatrix},$$

$$F_\xi = \begin{bmatrix} \tilde{A} \\ \vdots \\ \tilde{A}^{N_{\mathrm{p}}} \end{bmatrix},$$

$$G_\xi = \begin{bmatrix} \tilde{B} & & 0 \\ \vdots & \ddots & \\ \tilde{A}^{N_{\mathrm{p}}-1}\tilde{B} & \cdots & \tilde{B} \end{bmatrix},$$

$$D_\xi = \begin{bmatrix} \tilde{D} \\ \vdots \\ \tilde{A}^{N_{\mathrm{p}}-1}\tilde{D} + \tilde{A}^{N_{\mathrm{p}}-2}\tilde{D} + \cdots + \tilde{D} \end{bmatrix}.$$

Similar deductions can be made based on the output equation in (7) and (8), leading to:

$$\Psi(k) = F_\eta\boldsymbol{\xi}(k) + G_\eta\Delta U(k) + D_\eta, \tag{9}$$

where

$$\Psi(k) = \begin{bmatrix} \boldsymbol{\eta}(k+1) \\ \vdots \\ \boldsymbol{\eta}\left(k+N_{\mathrm{p}}\right) \end{bmatrix},$$

$$F_\eta = \begin{bmatrix} \tilde{C}\tilde{A} \\ \vdots \\ \tilde{C}\tilde{A}^{N_{\mathrm{p}}} \end{bmatrix},$$

$$G_\eta = \begin{bmatrix} \tilde{C}\tilde{B} & & 0 \\ \vdots & \ddots & \\ \tilde{C}\tilde{A}^{N_{\mathrm{p}}-1}\tilde{B} & \cdots & \tilde{C}\tilde{A}^{N_{\mathrm{p}}-N_{\mathrm{c}}}\tilde{B} \end{bmatrix},$$

$$D_\eta = \begin{bmatrix} \tilde{C}\tilde{D} \\ \vdots \\ \tilde{C}(\tilde{A}^{N_{\mathrm{p}}-1}\tilde{D} + \tilde{A}^{N_{\mathrm{p}}-2}\tilde{D} + \cdots + \tilde{D}) \end{bmatrix}.$$

2) DESIGN OF OBJECTIVE FUNCTION

To avoid collisions between carriages during URTT operation, this paper sets the control objective as maintaining a safe distance between train carriages and keeping their relative speed close to zero. This ensures distance safety and synchronized speeds between individual carriages. Thus, the desired safe distance between carriages and the target relative speed are defined as

$$\boldsymbol{w}_{\mathrm{r}} = \left[w_{x_1}, \cdots, w_{x_{n,n-1}}, w_{v_1}, \cdots, w_{v_{n,n-1}}\right]^\top,$$

where $w_{x_{2,1}}$ to $w_{x_{n,n-1}}$ represent the relative distance between the individual carriages and $w_{v_{2,1}}$ to $w_{v_{n,n-1}}$ represent the relative speed between carriages.

Therefore, the primary control objectives of this paper are to ensure the displacement and speed tracking accuracy of the train's first carriage, along with the ability to track the desired relative distances and relative speed between carriages. This involves optimizing the deviations in system state variables and control inputs. Additionally, to avoid excessive traction and braking variations, the design objective function is formulated as follows:

$$J = \sum_{k=1}^{N_{\mathrm{p}}} \|W(k) - \Psi(k)\|_Q^2 + \sum_{k=1}^{N_{\mathrm{c}}} \|\Delta U(k)\|_R^2, \tag{10}$$

where $W(k) = \left[\mathbf{w}_{\mathrm{r}}(k+1)\ldots\mathbf{w}_{\mathrm{r}}(k+N_{\mathrm{p}})\right]$ represents the vector representation of the desired output, and Q and R are output and control weighting matrices of appropriate dimensions. The first term on the right-hand side of (10) reflects the system's ability to track the desired relative distances and relative speed between carriages

and the reference trajectory. The second term represents the requirement for smooth variations in control inputs.

3) DESIGN OF CONSTRAINTS

Further, after the objective function of predictive control is designed, the following constraints should be considered to ensure the smooth, safe, and precise speed control and station stopping control of the train:

$$0 \le x_1 \le x_{\max}, \tag{11}$$

$$-l_{\mathrm{d}} - l_{\mathrm{safe}} \le x_{(2,\ldots,n),k} \le l_{\mathrm{d}} + l_{\mathrm{safe}}, \tag{12}$$

$$0 \le v_1 \le v_{\max}, \tag{13}$$

$$u_{\min} \le u_{1,\ldots,n} \le u_{\max}, \tag{14}$$

$$\Delta u_{\min} \le \Delta u_{1,\ldots,n} \le \Delta u_{\max}. \tag{15}$$

In (11), $x_{\max}$ represents the station stopping point, ensuring the train can come to a stop at the appropriate position aligning with the platform screen doors. In (12), $x_{(2,\ldots,n),k}$ denotes the relative distance between adjacent carriages, l_{d} is the desired distance between each carriages, and l_{safe} represents the maximum possible relative distance. In (13), $v_{\max} = \min\{v_{\mathrm{l}}, v_{\mathrm{p}}, v_{\mathrm{t}}\}$, where v_{l} is the maximum allowable speed determined by track conditions, v_{p} is the speed limit from the ATP profile, and v_{t} is design speed limit of trains. In (14), $u_{\min}$ and $u_{\max}$ represent the output minimum and maximum traction forces achievable due to physical limitations of the traction motors. In (15), $\Delta u_{\max}$ represents the maximum allowable change in traction force, and $\Delta u_{\min}$ represents the maximum allowable change in braking force.

In summary, setting $N_p = N_c = N$, the optimization model for the train speed predictive control is given

$$\begin{aligned}
&\min J = \sum_{k=1}^{N_{\mathrm{p}}} \|W(k) - \Psi(k)\|_Q^2 + \|\Delta U(k)\|_R^2 \\
&\text{s.t. } \boldsymbol{\xi}(k+1) = \tilde{A}\boldsymbol{\xi}(k) + \tilde{B}\Delta\boldsymbol{u}(k) + \tilde{D} \\
&\quad 0 \le x_1 \le x_{\max} \\
&\quad 0 \le v_1 \le v_{\max} \\
&\quad u_{\min} \le u_{1,\ldots,n} \le u_{\max} \\
&\quad \Delta u_{\min} \le \Delta u_{1,\ldots,n} \le \Delta u_{\max} \\
&\quad -l_{\mathrm{d}} - l_{\mathrm{safe}} \le x_{(2,\ldots,n),k} \le l_{\mathrm{d}} + l_{\mathrm{safe}}.
\end{aligned} \tag{16}$$

B. DESIGN OF STABILITY-ENHANCED MODEL PREDICTIVE CONTROL

The prediction horizon N is the number of future control intervals that the MPC controller must evaluate through prediction while optimizing its cost function at control interval k. A larger N increases computational costs, while a smaller N can lead to instability. We introduce a terminal cost to address this issue and propose an SEMPC approach. The cost function needs to be modified to account for computations up to infinity to build a stable MPC. Assuming the error vector at each time sample is $Y(k) = W(k) - \Psi(k)$, this modification can be expressed as

$$\sum_{k=1}^{\infty} \left(\|Y(k)\|_Q^2 + \|\Delta U(k)\|_R^2 \right).$$

By dividing the cost function into two terms, we obtain:

$$\begin{aligned}
J = &\sum_{k=1}^{N} \left(Y(k)^\top Q Y(k) + \Delta U(k)^\top R \Delta U(k) \right) \\
&+ \sum_{k=N+1}^{\infty} \left(Y(k)^\top Q Y(k) + \Delta U(k)^\top R \Delta U(k) \right).
\end{aligned}$$

It can also be expressed as

$$J = \sum_{k=1}^{N} \left(Y(k)^\top Q Y(k) + \Delta U(k)^\top R \Delta U(k) \right) + J^*,$$

where

$$\begin{aligned}
J^* = \sum_{j=0}^{\infty} \big[&Y(N+1+j)^\top Q Y(N+1+j) \\
&+ \Delta U(N+1+j)^\top R \Delta U(N+1+j) \big].
\end{aligned}$$

Due to the presence of the feedback control law $\Delta U(N+1+j) = KY(N+1+j)$, it can be derived that

$$\begin{aligned}
J^* = \sum_{j=0}^{\infty} \big[&(Y(N+1+j)^\top Q Y(N+1+j) \\
&+ Y(N+1+j)^\top K^\top R K Y(N+1+j) \big].
\end{aligned}$$

After simplification, it can be obtained that

$$J^* = \sum_{j=0}^{\infty} \left(Y(N+1+j)^\top \left(Q + K^\top R K \right) Y(N+1+j) \right). \tag{17}$$

Also, one has

$$Y(N+1+j) = (\tilde{A} + \tilde{B}K)^j Y(N+1). \tag{18}$$

Substituting (18) into (17), we get

$$\begin{aligned}
J^* = \sum_{j=0}^{\infty} \big[&Y(N+1)^\top \left((\tilde{A} + \tilde{B}K)^j \right)^\top \\
&\times \left(Q + K^\top R K \right) (\tilde{A} + \tilde{B}K)^j Y(N+1) \big].
\end{aligned} \tag{19}$$

Let

$$P = \sum_{j=0}^{\infty} \left(\left((\tilde{A} + \tilde{B}K)^j \right)^\top \left(Q + K^\top R K \right) (\tilde{A} + \tilde{B}K)^j \right).$$

Substituting this into (19) and rearranging, we obtain:

$$J^* = Y(N+1)^\top P Y(N+1).$$

Finally, the objective function of the SEMPC controller can be expressed as

$$J = \sum_{k=1}^{N} \left(Y(k)^\top Q Y(k) + \Delta U(k)^\top R \Delta U(k) \right) + Y(N+1)^\top P Y(N+1). \quad (20)$$

For the solution of P, we utilize the following equation to solve the Linear Matrix Inequality (LMI) optimization problem, where there are readily available efficient computational tools for LMI problems [11], [41]:

$$P = \left(Q + K^\top R K \right) + \left((\tilde{A} + \tilde{B}K)^j \right)^\top \left(Q + K^\top R K \right) (\tilde{A} + \tilde{B}K)^j.$$

Quadratic programming is widely used for solving constrained optimization problems in predictive control. Therefore, this paper transforms the constrained optimization problem in (16) into quadratic programming. Substituting (8) into the optimization objective in (20) and disregarding the constant terms, we obtain:

$$J = \Delta U(k)^\top \left(G_\eta^\top \bar{Q} G_\eta + \tilde{R} \right) \Delta U(k) + 2 \left[E^\top \bar{Q} G_\eta - W(k)^\top \bar{Q} G_\eta + D_\eta^\top \bar{Q} G_\eta \right] \Delta U(k), \quad (21)$$

where

$$\bar{Q} = \begin{bmatrix} \tilde{Q} & \\ & P \end{bmatrix},$$

$\tilde{Q} = I_{N_\mathrm{p}} \otimes Q$, $\tilde{R} = I_{N_\mathrm{c}} \otimes R$, and $\otimes$ represents the Kronecker product. Furthermore, let $H = {G_\eta}^\top \bar{Q} G_\eta + \tilde{R}$, and $\boldsymbol{g} = {G_\eta}^\top \bar{Q} \left[F_\eta \xi(k) - W(k) + D_\eta \right]$, then (21) can be rearranged as

$$J = \frac{1}{2} \Delta U(k)^\top H \Delta U(k) + \boldsymbol{g}^\top U(k).$$

After obtaining the quadratic form of the objective function, constraints need to be transformed into the form of control increments, as the control increments within the control domain are considered variables to be solved. Therefore, the constraint part of (16) can be organized as follows:

$$\boldsymbol{\xi}_{\min} \le Z \boldsymbol{\xi}(k+1+i) \le \boldsymbol{\xi}_{\max}, \quad (22)$$

$$\boldsymbol{u}_{\min} \le \boldsymbol{u}(k+i) \le \boldsymbol{u}_{\max}, \quad (23)$$

$$\Delta \boldsymbol{u}_{\min} \le \Delta \boldsymbol{u}(k+i) \le \Delta \boldsymbol{u}_{\max}, \quad (24)$$

where $i = 0, 1, \cdots, N-1$.

In (22), $Z = \begin{bmatrix} I_{(n+1)\times(n+1)} & O_{(n+1)\times(2n-1)} \end{bmatrix}$ ensures that constraints on train displacement, inter-carriage distances, and train speed. $\xi_{\min}$ represents the minimum values for train displacement, the minimum expected inter-carriage distance, and the minimum train speed, defined as

$$\boldsymbol{\xi}_{\min} = \begin{bmatrix} 0 & \boldsymbol{l}_{\min}^\top & 0 \end{bmatrix}_{1\times(n+1)}^\top,$$

where $\boldsymbol{l}_{\min} = [\, l_\mathrm{d} + l_{\text{safe}} \quad \cdots \quad l_\mathrm{d} + l_{\text{safe}} \,]_{1\times(n-1)}^\top$.

Similarly, $\xi_{\max}$ represents the maximum values for train displacement, the maximum inter-carriage distance, and the maximum train speed, defined as

$$\boldsymbol{\xi}_{\max} = \begin{bmatrix} x_{\max} & \boldsymbol{l}_{\max}^\top & v_{\max} \end{bmatrix}_{1\times(n+1)}^\top,$$

where $\boldsymbol{l}_{\max} = [l_\mathrm{d} + l_{\text{safe}} \quad \cdots \quad l_\mathrm{d} + l_{\text{safe}}]_{1\times(n-1)}^\top$.

Then within the prediction horizon, as indicated by (12), the constraint can be expressed as

$$\Xi_{\min} \le \tilde{A}_\mathrm{p} \Xi(k) + \tilde{B}_\mathrm{p} \Delta U(k) + \tilde{D}_\mathrm{p} \le \Xi_{\max}, \quad (25)$$

where $\tilde{A}_\mathrm{p} = I_{N_\mathrm{p}} \otimes Z\tilde{A}$, $\tilde{B}_\mathrm{p} = I_{N_\mathrm{c}} \otimes Z\tilde{B}$, and $\tilde{D}_\mathrm{p} = \mathbf{1}_{N_\mathrm{p}} \otimes Z\tilde{D}$, where $\mathbf{1}_{N_\mathrm{p}}$ is a column vector with N_p rows. $\Xi_{\min}$ and $\Xi_{\max}$ represent the sets of minimum and maximum values for train displacement, inter-carriage distances, and train speed within the prediction horizon.

In (23), $\boldsymbol{u}_{\min}$ and $\boldsymbol{u}_{\max}$ denote the sets of minimum and maximum traction forces applied to each carriage of the train at the current moment, respectively.

$$\boldsymbol{u}_{\min} = \begin{bmatrix} u_{\min_1} & \cdots & u_{\min_n} \end{bmatrix}_{1\times n}^\top,$$

$$\boldsymbol{u}_{\max} = \begin{bmatrix} u_{\max_1} & \cdots & u_{\max_n} \end{bmatrix}_{1\times n}^\top.$$

There is the following relationship between control inputs and control increments:

$$\boldsymbol{u}(k+i) = \boldsymbol{u}(k+i-1) + \Delta \boldsymbol{u}(k+i), \quad i = 0, 1, \cdots, N-1$$

Therefore, (23) can be represented in vector form:

$$U_{\min} \le U_t + L \Delta U(k) \le U_{\max}, \quad (26)$$

where $U_t = \mathbf{1}_{N_\mathrm{c}} \otimes \boldsymbol{u}(k-1)$,

$$L = \begin{bmatrix} I_{n\times n} & & \\ \vdots & \ddots & \\ I_{n\times n} & \cdots & I_{n\times n} \end{bmatrix}.$$

$\mathbf{1}_{N_\mathrm{c}}$ is a column vector with N rows; $\boldsymbol{u}(k-1)$ represents the actual control inputs at the previous time step. $U_{\min}$ and $U_{\max}$ are the sets of minimum and maximum values for control inputs within the control domain, respectively. $\Delta \boldsymbol{u}_{\min}$ and $\Delta \boldsymbol{u}_{\max}$ represent the sets of minimum and maximum changes in traction force applied to each carriage of the train at the current moment. They are represented as $\Delta \boldsymbol{u}_{\min} = \begin{bmatrix} \Delta u_{\min_1} & \cdots & \Delta u_{\min_n} \end{bmatrix}_{1\times n}^\top$ and $\Delta \boldsymbol{u}_{\max} = \begin{bmatrix} \Delta u_{\max_1} & \cdots & \Delta u_{\max_n} \end{bmatrix}_{1\times n}^\top$, respectively. In vector form, they can be represented as

$$\Delta U_{\min} \le \Delta U(k) \le \Delta U_{\max}, \quad (27)$$

where $\Delta U_{\min}$ and $\Delta U_{\max}$ represent the sets of minimum and maximum values for control increments within the control domain, respectively. Organizing the constraints from (25), (26), and (27), we can obtain:

$$F_\mathrm{p} \Xi(k) + G_\mathrm{p} \Delta U(k) \le M, \quad (28)$$

where

$$F_{\mathrm{p}}=\begin{bmatrix}\tilde{A}_{\mathrm{p}}\\ -\tilde{A}_{\mathrm{p}}\\ O\\ O\\ O\\ O\end{bmatrix},\quad G_{\mathrm{p}}=\begin{bmatrix}\tilde{B}_{\mathrm{p}}\\ -\tilde{B}_{\mathrm{p}}\\ L\\ L\\ I_{n\cdot N_{\mathrm{c}}}\\ I_{n\cdot N_{\mathrm{c}}}\end{bmatrix},M=\begin{bmatrix}\Xi_{\max}-\tilde{D}_{\mathrm{p}}\\ -\left(\Xi_{\min}-\tilde{D}_{\mathrm{p}}\right)\\ U_{\max}\\ -U_{\min}\\ \Delta U_{\max}\\ \Delta U_{\min}\end{bmatrix}.$$

The zero matrix O has dimensions $(n\cdot N_{\mathrm{p}})\times(3n\cdot N_{\mathrm{p}})$, $I_{n\cdot N_{\mathrm{c}}}$ is the identity matrix with dimensions $n\cdot N_{\mathrm{c}}$. Further, substituting (8) into (28) and organizing the constraints, we get:

$$F_{\mathrm{p}}F_{\xi}\xi(k)+\left(F_{\mathrm{p}}G_{\xi}+G_{\mathrm{p}}\right)\Delta U(k)+F_{\mathrm{p}}D_{\xi}-M\leq\mathbf{0}.$$

Finally, the design of the SEMPC for URTT can be formulated as follows:

$$\begin{aligned}\min\quad & J=\frac{1}{2}\Delta U(k)^{\top}H\Delta U(k)+\boldsymbol{g}^{\top}U(k)\\ \text{s.t. }& F_{\mathrm{p}}F_{\xi}\xi(k)+\left(F_{\mathrm{p}}G_{\xi}+G_{\mathrm{p}}\right)\Delta U(k)+F_{\mathrm{p}}D_{\xi}-M\leq\mathbf{0}.\end{aligned}\tag{29}$$

After solving the optimization problem within each control cycle, a series of control input increments within the control domain is obtained:

$$\Delta U^{*}(k)=\begin{bmatrix}\Delta u^{*}(k)\\ \Delta u^{*}(k+1)\\ \cdots\\ \Delta u^{*}\left(k+N_{\mathrm{c}}-1\right)\end{bmatrix}.$$

The first element of this control sequence is applied as the actual control input increment to the system, i.e.,

$$\boldsymbol{u}(k)=\boldsymbol{u}(k-1)+\Delta\boldsymbol{u}^{*}(k).$$

In the next control cycle, the above process is repeated, thus cyclically achieving the SEMPC of the train.

IV. EXPERIMENT VERIFICATION

The data used in this paper is sourced from operational data from a specific urban rail line. Further, a six-carriage train composition is chosen, employing a D-type train model, with specific parameters provided by the vehicle manufacturer, as shown in Table 1 [25] is assumed that the speed and displacement information of the train is obtained through sensors, and the actuators are considered to be healthy and free of faults.

This paper compares and analyzes the control performance of three different algorithms in three scenarios: the MPC algorithm, the AFSMC algorithm, and the SEMPC approach. The three scenarios include the single-section, multi-section, and disturbance train operation scenarios. The first scenario is a typical train operation control scenario with a relatively short overall operation time and distance. The second scenario is the multi-section train operation scenario, which includes three operation sections, three station stopping, and a longer overall operation time and distance, posing a challenge to the overall stability of the train's operation control.

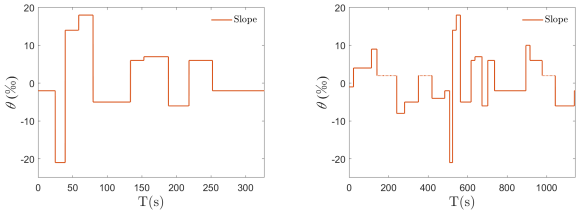

(a) (b)

FIGURE 3. Slope changes in (a) single-section train operation scenarios and (b) multi-section train operation scenarios.

TABLE 1. Parameters of train.

Parameters	Value
m_i (t)	64.8
c_0 (N/t)	9.888
c_1 (Ns/mt)	0.005
c_2 (Ns^2/m^{2}t)	0.00195
k_s (N/m)	10^7
l (m)	1.2
l_{safe} (m)	0.2
$u_{\max}$ (N)	7×10^4
$u_{\min}$ (N)	-6.5×10^4
$\Delta u_{\max}$ (N/s)	6×10^4
$\Delta u_{\min}$ (N/s)	-6×10^4

The m_i is the load weight without passengers.

The last one is a train operation scenario with disturbance, which simulates the train scenario switching from indoor to outdoor and verifies the performance of different algorithms with disturbances.

The control performance metrics are analyzed based on four aspects: input cost, speed error, displacement error, and station-stopping error. The calculation methods for performance metrics are given

$$\begin{aligned}\mathrm{E}_u&=\sum_{i=1}^{n}\int u_i^2\mathrm{d}t,\\ \mathrm{E}_v&=\frac{\sum_{k=0}^{T}\left|v_{\mathrm{r}}(k)-v_1(k)\right|}{T},\\ \mathrm{E}_x&=\frac{\sum_{k=0}^{T}\left|x_{\mathrm{r}}(k)-x_1(k)\right|}{T},\\ \mathrm{E}_{\mathrm{p}}&=\left|x_1^{\mathrm{desire}}-x_1^{\mathrm{end}}\right|.\end{aligned}$$

A. SINGLE-SECTION TRAIN OPERATION SCENARIO

The first scenario is the single-section train operation scenario, aiming to validate the performance of the proposed algorithm in a short-distance operation scenario with only one operating section. This scenario includes performance metrics related to train speed control, train displacement control, inter-carriage distance, speed control, and station stopping error. Additionally, to assess the control performance of the algorithm in terms of the instantaneous traction and braking force variation rate of train motors, which is crucial for riding comfort, this paper sets the acceleration phase in the

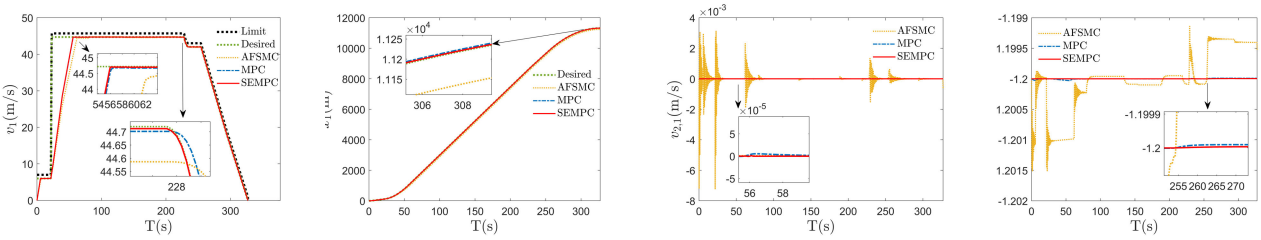

FIGURE 4. Performance comparison of different algorithms in the single-section train operation scenario, including (a) speed profile tracking, (b) displacement profile tracking, (c) inter-carriage relative distance, and (d) inter-carriage relative speed.

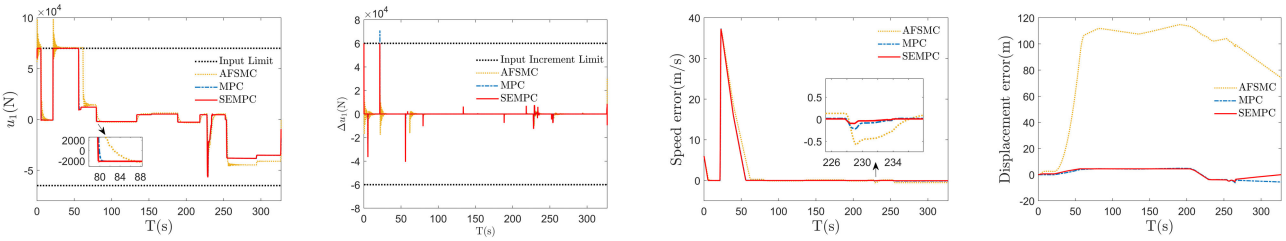

FIGURE 5. Performance comparison of different algorithms in the single-section train operation scenario, including (a) input curve, (b) input increment curve, (c) speed error curve, and (d) displacement error curve.

expected speed profile as the phase with the maximum target speed. The expected profile does not explicitly consider the instantaneous traction and braking force variation rate of train motors. Furthermore, the simulation includes time-varying slope resistance to evaluate the control effectiveness in the presence of time-varying slope resistance within the section. In this simulation, $N = N_{\mathrm{p}} = N_{\mathrm{c}} = 3$. The control and output weighting matrices are set as follows:

$$Q = \mathrm{diag}([0.5, 10^{12}, 10^{12}, 10^{12}, 10^{12}, 10^{12}, 10^{9}, 10^{12}, 10^{12}, 10^{12}, 10^{12}, 10^{12}, 0, 0, 0, 0, 0, 0]),$$

$$R = 10^{-5} \times \mathrm{diag}([1, 1, 1, 1, 1, 1]),$$

where $\mathrm{diag}(\cdots)$ denotes the diagonalization operation. Figure 4 presents the performance comparison results of the MPC, AFSMC, and algorithm proposed in this paper. The performance metrics comparison for the three algorithms are summarized in Table 2.

Figure 4(a) displays the speed control performance of the train's first carriage, where the train adheres to the maximum safe operating speed. The thick black dashed line represents the train overspeed protection curve, and the maximum safe operating speed limit during this period is 45.8 m/s. The graph shows that the SEMPC approach achieves the most accurate and stable speed tracking of the expected speed profile, considering riding comfort. The speed tracking performance is significantly improved. Figure 4(b) illustrates the displacement control curve of the train's first carriage. It can be observed from the graph that the SEMPC approach effectively enhances the displacement tracking accuracy. Figures 4(c) and 4(d) represent the relative speed and relative distance between the first and second carriages of the train, respectively. These figures demonstrate that the SEMPC approach excels in controlling the relative speed and relative distance between carriages to ensure safe train operation.

TABLE 2. The performance comparison of different algorithms in single-section scenario.

Algorithm	E_u (10^{12}N)	E_v (m/s)	E_d (m)	E_p (m)
SEMPC	**1.8197**	**1.9123**	**3.3014**	**0.004**
MPC	1.8117	1.9365	3.7862	5.596
AFSMC	1.6799	2.4046	89.5023	74.098

Figures 5(a) and 5(b) depict the changes in traction/braking forces and traction/braking variation rates during the train operation process. In Fig. 5(a), both SEMPC and MPC algorithms control the traction/braking forces, ensuring they remain within the constraints of the traction/braking control unit's output performance. However, in Fig. 5(b), the MPC algorithm fails to control the traction change within the constraints, unlike the SEMPC approach. the SEMPC approach adapts to the performance of the traction/braking control unit, ensuring that traction/braking variation rates remain within the constraints throughout the train operation. Finally, Figs. 5(c) and 5(d) display the speed error curve and displacement error curve during the train operation process. These figures show that the SEMPC approach effectively reduces both speed and displacement errors. It rapidly maintains errors close to zero after sharp changes in the expected curve, resulting in the lowest average speed and displacement errors. Combined with the results presented in Table 2, it is evident that the proposed algorithm achieves better control performance with lower average speed and displacement errors. The distance from the train to the expected stopping point is only 0.004 m after the train comes

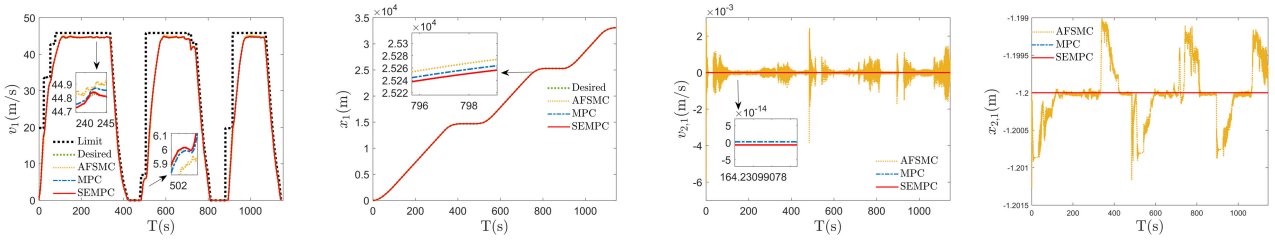

FIGURE 6. Performance comparison of different algorithms in the multi-section train operation scenario, including (a) speed profile tracking, (b) displacement profile tracking, (c) inter-carriage relative distance, and (d) inter-carriage relative speed.

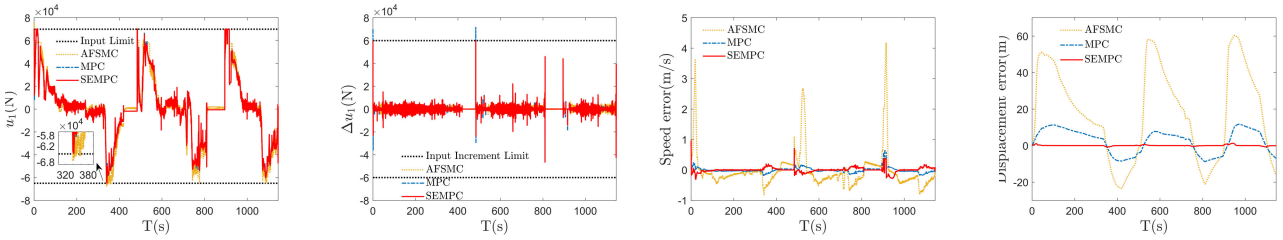

FIGURE 7. Performance comparison of different algorithms in the multi-section train operation scenario, including (a) input curve, (b) input increment curve, (c) speed error curve, and (d) displacement error curve.

to a stop, which is significantly better than the MPC and AFSMC algorithms. Additionally, the input cost is only 0.44% higher than the MPC algorithm or 8.32% higher than the AFSMC algorithm.

Consequently, the SEMPC approach exhibits precise, stable, and safe operational control, with the best control performance, as long as constraints such as traction/braking force and traction/braking force variation rates are met.

B. MULTI-SECTION TRAIN OPERATION SCENARIO

The second scenario entails a multi-section train operation, aiming to validate the algorithm's performance in a real-world scenario encompassing multiple operating sections over long distances. The overspeed protection curve, expected trajectory, and slope data in this scenario are derived from real onboard data of an urban rail line. Both the overspeed protection curve and the desired trajectory are calculated by onboard equipment based on the actual environmental parameters of the railway route. The data in this multi-section train scenario exhibit complexity, unevenness, and nonlinearity. Consequently, achieving precise, smooth, and secure train operation control poses a significant challenge for ATO control. In this simulation, $N = N_p = N_c = 3$. The control and output weighting matrices are set as follows:

$$Q = \mathrm{diag}([0.05, 10^{12}, 10^{12}, 10^{12}, 10^{12}, 10^{12}, 50, 10^{12}, 10^{12}, 10^{12}, 10^{12}, 10^{12}, 0, 0, 0, 0, 0, 0]),$$
$$R = 10^{-8} \times \mathrm{diag}([1, 1, 1, 1, 1, 1]).$$

The performance metrics for the three algorithms are compared and presented in Table 3. Notably, the parking distances for the three sections are 14687 m for Section I, 25279 m for Section II, and 33086 m for Section III.

As shown in Fig. 6(a) and Fig. 6(b), when facing the expected speed profile of the train in the complex multi-section real-world scenario, the AFSMC algorithm exhibits unstable control, performing the worst. In contrast, the SEMPC and MPC algorithms can adequately track the expected trajectory, yet the SEMPC approach achieves superior precision. Figures 6(c) and 6(d) reveal that similar to the single-section train operation scenario, in the context of the complex multi-section real-world scenario, the SEMPC approach continues demonstrating outstanding control performance in inter-carriage relative speed and relative distance.

Figures 7(a) and 7(b) show that the AFSMC algorithm struggles to achieve train operation control under the constraints of traction and braking forces. The MPC algorithm faces challenges in controlling train operation under constraints on traction and braking force variations. Balancing the output performance of the traction control unit, the braking control unit, and riding comfort, the SEMPC approach performs superiorly compared to the other two algorithms. Figures 7(c) and 7(d) depict the train speed error curve and train displacement error curve in the complex multi-section real-world scenario. These figures illustrate that the algorithm employed in this paper significantly reduces train speed and displacement errors at any stage in the real-world scenario compared to the other two algorithms. This achievement leads to minimal overall average speed and displacement errors.

Referring to the input costs in Table 3, it is evident that the SEMPC approach only requires a 0.67% increase in

TABLE 3. The performance comparison of different algorithms in multi-section scenario.

Algorithm	E_u	E_v (m/s)				E_d (m)				E_p (m)			
	(10^{12}N)	Sec 1	Sec 2	Sec 3	average	Sec 1	Sec 2	Sec 3	average	Sec 1	Sec 2	Sec 3	average
SEMPC	**4.5657**	**0.0341**	**0.0369**	**0.0721**	**0.0447**	**0.1048**	**0.0832**	**0.2377**	**0.1309**	**0.020**	**0.049**	**0.043**	**0.037**
MPC	4.5349	0.0450	0.0512	0.0843	0.0571	7.1993	5.4799	6.8170	6.4974	8.461	8.730	6.849	8.013
AFSMC	4.0438	0.2750	0.3829	0.4802	0.3649	24.7635	24.8800	29.3763	25.9727	23.479	20.917	15.814	20.070

TABLE 4. The performance comparison of different algorithms with disturbance.

Algorithm	Constant Disturbance				Harmonic Disturbance			
	E_u (10^{12}N)	E_v (m/s)	E_d (m)	E_p (m)	E_u (10^{12}N)	E_v (m/s)	E_d (m)	E_p (m)
SEMPC	**1.7776**	**0.0165**	**0.1093**	**0.0881**	**1.5465**	**0.0165**	**0.0046**	**0.00005**
MPC	1.9669	0.0280	0.8296	0.6645	1.7782	0.1159	0.8340	0.3180
AFSMC	5.5444	0.7494	65.5300	31.7175	2.7902	0.6655	56.8689	25.6186

input costs compared to the MPC algorithm. Meanwhile, it achieves a 21.71% improvement in average speed error precision, a twofold enhancement in average displacement error precision, and a 99.53% improvement in stopping error precision. On the other hand, compared to the AFSMC algorithm, the SEMPC approach incurs a 12.91% increase in input costs, and the average speed error and average displacement error are respectively 0.12 times and 0.005 times those of the AFSMC algorithm. Moreover, the stopping error is 0.0018 times that of the AFSMC algorithm.

In summary, in a multi-section train operation scenario, the SEMPC approach outperforms the MPC and AFSMC algorithms, ensuring superior train control, ensuring safe, punctual, efficient, and smooth train operation while adhering to constraints on traction, braking forces, and their variations.

C. TRAIN OPERATION SCENARIO WITH DISTURBANCE

Considering that trains will encounter different types of wind disturbances when operating in the open air. This paper conducts a thorough comparison of the proposed SEMPC approach with other control algorithms to validate its performance in the train operation scenario with disturbance. Specifically, we conducted the experiments to verify the performance of the algorithm with different kinds of wind disturbances. The two groups of wind disturbances are constant disturbance and harmonic disturbance respectively. The former uses the stable wind model of the train in the operating process [42], while the latter is a kind of model of the gust, which can approximately reveal the action process of wind disturbance on the train [43]. The change of disturbance is shown in Fig. 8. The performance metrics for the three algorithms with disturbance are compared and presented in Table 4.

1) CONSTANT DISTURBANCE

In this case, the constant disturbance is used as the stable wind model, and the disturbance model is as follows

$$\hat{w} = 0.2,$$

where $\hat{w}$ represents the disturbance in train operation scenario. The comparison of different algorithms with constant disturbance is shown in Fig. 9.

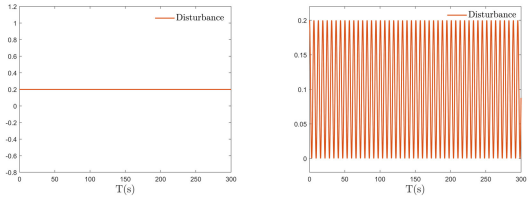

FIGURE 8. Change of (a) constant disturbance and (b) nonlinear disturbance in train operation scenario.

In Fig. 9, this paper shows four evolutions, such as relative distance, relative speed, speed error and displacement error, which can reflect the stability of the algorithm. Combining Fig. 9 with Table 4, it can be seen that the SEMPC approach can keep the relative distance no more than 0.0005 m and the relative speed no more than 0.001 m/s, and the overall change fluctuation is smaller than that of the compared methods, showing the superior performance of the proposed approach with constant disturbance. On the other hand, the average displacement error of the proposed approach is kept at 0.1093 m, the average speed error is kept at 0.0165 m/s, and the parking accuracy is 0.0881 m. It can be seen that the SEMPC approach shows the best performance with constant disturbance in control accuracy and stability.

2) NONLINEAR DISTURBANCE

In this case, a gust model in harmonic form is used as a nonlinear disturbance, and the specific wind characteristics are as follows:

$$\hat{w} = 0.1 + 0.1 * \cos(t),$$

where $\hat{w}$ represents the harmonic disturbance in train operation scenario. The comparison of different algorithms with harmonic disturbance is shown in Fig. 10.

As can be seen from Fig. 10, the influence of harmonic disturbance on train operation is greater than that of constant disturbance. Nevertheless, the SEMPC approach performs well and can maintain accurate and stable control of trains under safety constraints. To be specific, in Figs. 10(a) and (b), the control of relative distance and relative speed of the other two algorithms with disturbance fluctuates violently,

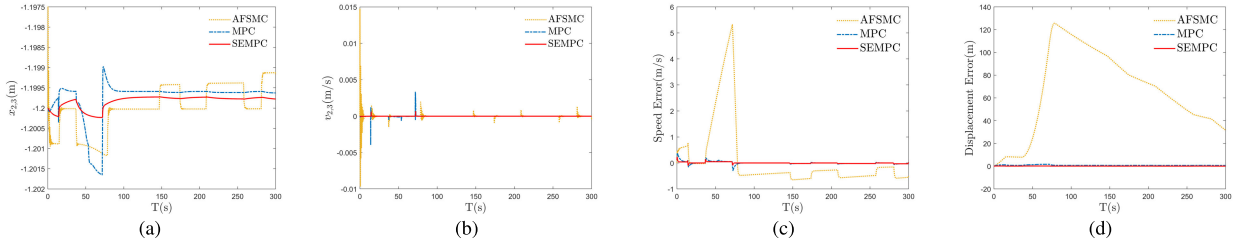

FIGURE 9. Performance comparison of different algorithms with constant disturbance, including (a) inter-carriage relative distance, (b) inter-carriage relative speed, (c) speed error curve, and (d) displacement error curve.

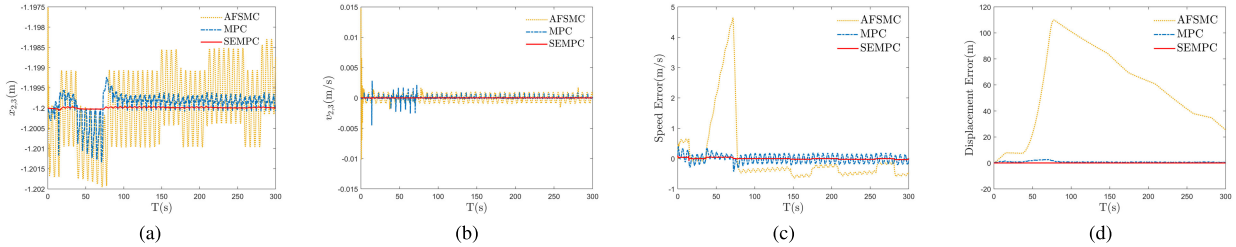

FIGURE 10. Performance comparison of different algorithms with nonlinear disturbance, including (a) inter-carriage relative distance, (b) inter-carriage relative speed, (c) speed error curve, and (d) displacement error curve.

but the performance of the SEMPC approach fluctuates slightly. This means that the SEMPC approach achieves stable and safe ATO control under nonlinear disturbance. As can be seen from Fig. 10(c) and (d), in the train operation scenario with nonlinear disturbance, the average speed error and average displacement error of the SEMPC approach also perform well, and the fluctuation is small. Combined with Table 4, it can be seen that the SEMPC approach performs better than the other algorithms with harmonic disturbance, and the accuracy of control is highest. In general, the proposed SEMPC approach can deal with disturbances and ensure the safe operation of trains in practical application.

V. CONCLUSION

In this paper, a stability-enhanced model predictive control approach tailored for urban rail transit trains has been developed. This approach has comprehensively accounted for the nonlinear characteristics of train operations and the intricate constraints within the track design. Through the proposed approach, it has achieved precise control over both train speed and station stopping while guaranteeing the relative speed and distance between train carriages. Experimental results have validated the algorithm's ability to ensure safe, punctual, efficient, and smooth train operations across diverse scenarios. However, this paper assumes that each carriage of the train can be controlled independently and different carriages follow the corresponding trajectory to achieve ATO control, which requires better hardware conditions and communication efficiency of equipment, and its cost will further increase. Therefore, in the future, we hope to simplify the algorithm so that it can be integrated into the onboard equipment of urban rail transit trains and its performance can be verified in practice.

REFERENCES

[1] J. Yin, T. Tang, L. Yang, J. Xun, Y. Huang, and Z. Gao, "Research and development of automatic train operation for railway transportation systems: A survey," *Transp. Res. C, Emerg. Technol.*, vol. 85, pp. 548–572, Dec. 2017.

[2] B. Ning, T. Tang, Z. Gao, F. Yan, F.-Y. Wang, and D. Zeng, "Intelligent railway systems in China," *IEEE Intell. Syst.*, vol. 21, no. 5, pp. 80–83, Sep. 2006.

[3] X. Dai, H. Zhao, S. Yu, D. Cui, Q. Zhang, H. Dong, and T. Chai, "Dynamic scheduling, operation control and their integration in high-speed railways: A review of recent research," *IEEE Trans. Intell. Transp. Syst.*, vol. 23, no. 9, pp. 13994–14010, Sep. 2022.

[4] Q. Wu, X. Ge, Q.-L. Han, B. Wang, H. Wu, C. Cole, and M. Spiryagin, "Dynamics and control simulation of railway virtual coupling," *Vehicle Syst. Dyn.*, vol. 61, no. 9, pp. 2292–2316, Sep. 2023.

[5] C. Jia, H. Xu, and L. Wang, "Nonlinear hybrid multipoint model of high-speed train with traction/braking dynamic and speed estimation law," *Math. Problems Eng.*, vol. 2019, pp. 1–14, Jan. 2019.

[6] H. Tang, Q. Wang, and X. Feng, "Robust stochastic control for high-speed trains with nonlinearity, parametric uncertainty, and multiple time-varying delays," *IEEE Trans. Intell. Transp. Syst.*, vol. 19, no. 4, pp. 1027–1037, Apr. 2018.

[7] D. He, L. Zhang, S. Guo, Y. Chen, S. Shan, and H. Jian, "Energy-efficient train trajectory optimization based on improved differential evolution algorithm and multi-particle model," *J. Cleaner Prod.*, vol. 304, Jul. 2021, Art. no. 127163.

[8] Q. Pu, X. Zhu, R. Zhang, J. Liu, D. Cai, and G. Fu, "Speed profile tracking by an adaptive controller for subway train based on neural network and PID algorithm," *IEEE Trans. Veh. Technol.*, vol. 69, no. 10, pp. 10656–10667, Oct. 2020.

[9] L. Yan, Y. Gao, Z. Yuan, H. Zhao, and S. Gao, "Robust PI protective tracking control of decentralized-power trains with model uncertainties against over-speed and signal passed at danger," *IET Control Theory Appl.*, vol. 15, no. 10, pp. 1314–1334, Jul. 2021.

[10] K. Zhou, S. Song, A. Xue, K. You, and H. Wu, "Smart train operation algorithms based on expert knowledge and reinforcement learning," *IEEE Trans. Syst., Man, Cybern., Syst.*, vol. 52, no. 2, pp. 716–727, Feb. 2022.

[11] X. Chen, X. Guo, J. Meng, R. Xu, S. Li, and D. Li, "Research on ATO control method for urban rail based on deep reinforcement learning," *IEEE Access*, vol. 11, pp. 5919–5928, 2023.

[12] G. Li, S. W. Or, and K. W. Chan, "Intelligent energy-efficient train trajectory optimization approach based on supervised reinforcement learning for urban rail transits," *IEEE Access*, vol. 11, pp. 31508–31521, 2023.

[13] L. Zhu, C. Shen, X. Wang, H. Liang, H. Wang, and T. Tang, "A learning based intelligent train regulation method with dynamic prediction for the metro passenger flow," *IEEE Trans. Intell. Transp. Syst.*, vol. 24, no. 4, pp. 3935–3948, Apr. 2023.
[14] W. Wang, J. Le, Z. Wang, X. Luo, J. Kurths, M. Yuan, and Y. Ma, "Event-triggered consensus control for high-speed train with time-varying actuator fault," *IEEE Access*, vol. 8, pp. 50553–50564, 2020.
[15] X. Wang, Z. Xiao, M. Chen, P. Sun, Q. Wang, and X. Feng, "Energy-efficient speed profile optimization and sliding mode speed tracking for metros," *Energies*, vol. 13, no. 22, p. 6093, Nov. 2020.
[16] Y. Cao, Z.-C. Wang, F. Liu, P. Li, and G. Xie, "Bio-inspired speed curve optimization and sliding mode tracking control for subway trains," *IEEE Trans. Veh. Technol.*, vol. 68, no. 7, pp. 6331–6342, Jul. 2019.
[17] B. Liang and T. Zhang, "Fractional order nonsingular terminal sliding mode cooperative fault-tolerant control for high-speed trains with actuator faults based on grey wolf optimization," *IEEE Access*, vol. 11, pp. 63932–63946, 2023.
[18] Y. Guo, P. Sun, X. Feng, and K. Yan, "Adaptive fuzzy sliding mode control for high-speed train using multi-body dynamics model," *IET Intell. Transp. Syst.*, vol. 17, no. 2, pp. 450–461, Feb. 2023.
[19] Y. Chen, D. Huang, Y. Li, and X. Feng, "A novel iterative learning approach for tracking control of high-speed trains subject to unknown time-varying delay," *IEEE Trans. Autom. Sci. Eng.*, vol. 19, no. 1, pp. 113–121, Jan. 2022.
[20] Z. Li, C. Yin, H. Ji, and Z. Hou, "Constrained spatial adaptive iterative learning control for trajectory tracking of high speed train," *IEEE Trans. Intell. Transp. Syst.*, vol. 23, no. 8, pp. 11720–11728, Aug. 2022.
[21] Y. Chen, D. Huang, T. Huang, and N. Qin, "Tracking control via iterative learning for high-speed trains with distributed input constraints," *IEEE Access*, vol. 7, pp. 84591–84601, 2019.
[22] H. Liang, L. Zhu, F. R. Yu, and X. Wang, "A cross-layer defense method for blockchain empowered CBTC systems against data tampering attacks," *IEEE Trans. Intell. Transp. Syst.*, vol. 24, no. 1, pp. 501–515, Jan. 2023.
[23] H. Liang, L. Zhu, and F. R. Yu, "Collaborative edge intelligence service provision in blockchain empowered urban rail transit systems," *IEEE Internet Things J.*, vol. 11, no. 2, pp. 2211–2223, May 2024.
[24] Y. Li, L. Zhu, H. Wang, F. R. Yu, T. Tang, and D. Zhang, "Joint security and resources allocation scheme design in edge intelligence enabled CBTCs: A two-level game theoretic approach," *IEEE Trans. Intell. Transp. Syst.*, vol. 24, no. 12, pp. 13948–13961, Dec. 2023.
[25] C. Jia, H. Xu, and L. Wang, "Robust nonlinear model predictive control for automatic train operation based on constraint tightening strategy," *Asian J. Control*, vol. 24, no. 1, pp. 83–97, Jan. 2022.
[26] Y. Liufu, L. Jin, and S. Li, "Modified gradient projection neural network for multiset constrained optimization," *IEEE Trans. Ind. Informat.*, vol. 19, no. 9, pp. 9413–9423, Sep. 2023.
[27] Y. Liufu, L. Jin, M. Shang, X. Wang, and F.-Y. Wang, "ACP-incorporated perturbation-resistant neural dynamics controller for autonomous vehicles," *IEEE Trans. Intell. Vehicles*, early access, pp. 1–12, 2024, doi: 10.1109/TIV.2023.3348632.
[28] S. J. Qin and T. A. Badgwell, "A survey of industrial model predictive control technology," *Control Eng. Pract.*, vol. 11, no. 7, pp. 733–764, Jul. 2003.
[29] T. Xu, J. Liu, Z. Zhang, G. Chen, D. Cui, and H. Li, "Distributed MPC for trajectory tracking and formation control of multi-UAVs with leader–follower structure," *IEEE Access*, vol. 11, pp. 128762–128773, 2023.
[30] H. Liu, J. Sun, and K. W. E. Cheng, "A two-layer model predictive path-tracking control with curvature adaptive method for high-speed autonomous driving," *IEEE Access*, vol. 11, pp. 89228–89239, 2023.
[31] S. Li, L. Yang, and Z. Gao, "Distributed optimal control for multiple high-speed train movement: An alternating direction method of multipliers," *Automatica*, vol. 112, Feb. 2020, Art. no. 108646.
[32] C. Di Meo, M. Di Vaio, F. Flammini, R. Nardone, S. Santini, and V. Vittorini, "ERTMS/ETCS virtual coupling: Proof of concept and numerical analysis," *IEEE Trans. Intell. Transp. Syst.*, vol. 21, no. 6, pp. 2545–2556, Jun. 2020.
[33] L. Zhang and X. Zhuan, "Development of an optimal operation approach in the MPC framework for heavy-haul trains," *IEEE Trans. Intell. Transp. Syst.*, vol. 16, no. 3, pp. 1391–1400, Jun. 2015.
[34] L. Wang, H. Xu, C. Zou, and G. Yang, "Application of the model predictive control with constraint tightening for ATO system," *Int. J. Control Autom.*, vol. 8, no. 11, pp. 245–262, Nov. 2015.
[35] Z. Zhang, H. Song, H. Wang, L. Liu, and H. Dong, "A model predictive control strategy with switching cost functions for cooperative operation of trains," *Sci. China Inf. Sci.*, vol. 66, no. 7, Jul. 2023, Art. no. 172206.
[36] B. Chen, Z. Huang, R. Zhang, W. Liu, H. Li, J. Wang, Y. Fan, and J. Peng, "Data-driven Koopman model predictive control for optimal operation of high-speed trains," *IEEE Access*, vol. 9, pp. 82233–82248, 2021.
[37] W. Zhao, J. Ding, Q. Zhang, X. He, and W. Liu, "A distributed multiparticle precise stopping control model based on the distributed model predictive control algorithm for high-speed trains," *J. Dyn. Syst., Meas., Control*, vol. 145, no. 11, Nov. 2023, Art. no. 111001.
[38] J. Felez, Y. Kim, and F. Borrelli, "A model predictive control approach for virtual coupling in railways," *IEEE Trans. Intell. Transp. Syst.*, vol. 20, no. 7, pp. 2728–2739, Jul. 2019.
[39] J. Xun, J. Yin, R. Liu, F. Liu, Y. Zhou, and T. Tang, "Cooperative control of high-speed trains for headway regulation: A self-triggered model predictive control based approach," *Transp. Res. C, Emerg. Technol.*, vol. 102, pp. 106–120, May 2019.
[40] M. Alamir, "Contraction-based nonlinear model predictive control formulation without stability-related terminal constraints," *Automatica*, vol. 75, pp. 288–292, Jan. 2017.
[41] C. Phanlert, T. Botmart, W. Weera, and P. Junsawang, "Finite-time extended dissipativity analysis for generalized neural networks with discrete and distributed time-varying delays," *IEEE Access*, vol. 11, pp. 118144–118160, 2023.
[42] M. Faieghi, A. Jalali, and S. K.-E.-D.-M. Mashhadi, "Robust adaptive cruise control of high speed trains," *ISA Trans.*, vol. 53, no. 2, pp. 533–541, Mar. 2014.
[43] Z. Li, Z. Hou, R. Zhang, and C. Yin, "Robust point-to-point iterative learning control for high speed trains with model uncertainty and wind gust," *Asian J. Control*, vol. 24, no. 6, pp. 3522–3537, Nov. 2022.

XI WANG received the B.S. degree in rail transit signal and control from the North University of China, Taiyuan, Shanxi, China, in 2017, and the M.S. degree in information and communication engineering from Inner Mongolia University, Huhhot, Inner Mongolia, China, in 2021. He is currently pursuing the Ph.D. degree in traffic information engineering and control with China Academy of Railway Sciences, Beijing, China. His current research interests include automatic train operation, intelligent transportation systems, and model predictive control.

KEJIA XING received the Ph.D. degree in traffic information engineering and control from China Academy of Railway Sciences, Beijing, China, in 2004. His current technical title is Researcher. He guides students' scientific research as a Ph.D. Supervisor. In recent years, he has been engaged in the research, standard setting, product development, scientific experiment, and the popularization and application of the next generation train operation control technology of urban rail transit.

JIAN WANG received the B.S. degree in automation and the M.S. degree in traffic information engineering and control from Beijing Jiaotong University, Beijing, China, in 2005 and 2008, respectively, and the Ph.D. degree in traffic information engineering and control from China Academy of Railway Sciences. He is currently an Associate Researcher with the Signal and Communication Research Institute, China Academy of Railway Sciences, and an Information Technology Project Management Professional. His research interests include railway signal and communication, and railway intelligent control and dispatching.